DOI: 10.1002/ejic.200700706

Proton and Deuteron Exchange in TTB-Like $Na_{1.2}Nb_{1.2}W_{0.8}O_6$: Structural Characterization and Spectroscopic Study

M. Luisa Sanjuán,[a] Alois Kuhn,*[b] M. Teresa Azcondo,[b] and Flaviano García-Alvarado[b]

Keywords: Materials science / Ion exchange / Electron diffraction / IR spectroscopy / Raman spectroscopy

Proton- and deuteron-exchange reactions have been performed on $Na_{1.2}Nb_{1.2}W_{0.8}O_6$ with the tetragonal tungsten bronze (TTB) structure. Na^+/H^+ and Na^+/D^+ ion exchange occurs when aqueous nitric acid solutions are used as the exchanging agent. Up to two out of the three Na^+ ions are readily exchanged to yield crystalline powder samples. The ion-exchange reaction proceeds topotactically, in other words the basic TTB structure is retained, although X-ray and electron diffraction reveal that the exchange process produces an orthorhombic supercell which possesses a true unit cell based on $a \approx 2\sqrt{2}a_{TTB}$, $b \approx \sqrt{2}a_{TTB}$, c = 2TTB. The nature of the hydrogenated species has been analyzed by means of IR and Raman spectroscopy on both parent and exchanged compounds. The results are interpreted in terms of short M–O (M = Nb or W) bonds formed through the trapping of two protons or deuterons close to the oxygen ions of the [MO_6] octahedra. The band assigned to the short M–O bonds disappears after deprotonation.

Introduction

The name tetragonal tungsten bronzes (TTBs), which originally referred to the non-stoichiometric compounds K_xWO_3 (x = 0.4–0.6),[1] has been extended to all compounds showing the same features, i.e. structure and variable composition. A large number of functional materials with interesting properties from a technological point of view are currently known by this generic name.[2–6] As regards their structure, a regular corner-shared octahedral network is built up of MO_6 octahedra arranged as shown in Figure 1 to form five-, four-, and three-sided tunnels, labeled A, B, and C, respectively. Alkali-metal atoms are located in the first two types of tunnels (A and B).[1,7] The composition of the unit cell can be expressed by the formula $A_xW_{10}O_{30}$ ($x \leq 6$), where A is the ion located in the tunnels. Several cations of suitable charge and size, including alkaline-earth metals, can be accommodated in the tunnels with variable occupancies.[7,8] The $A_6W_{10}O_{30}$-type tungsten bronze (i.e. the x = 6 member), where both five- and four-sided tunnels are fully occupied, is called the *filled* tungsten bronze.

Attempts have been made to replace W by other metals such us Ta, Mo, or Nb.[9] Ikeda et al.,[8] for example, have studied the effects of substituting W for Nb ions in niobates with the TTB structure. The X-ray diffraction study of the

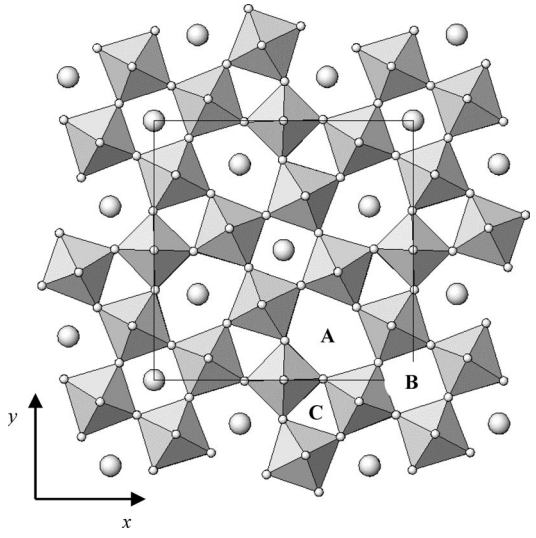

Figure 1. Schematic representation of the TTB structure projected onto the xy plane. Sodium: large circles; oxygen: small circles. MO_6 octahedra (M = Nb, W) are shown in grey.

$NaNbO_3$-Nb_2O_5-WO_3 system reported by Marinder[10] reveals the existence of phases related to the TTB structure. An investigation of the aforementioned system by means of high-resolution electron microscopy led to the discovery of several structural types related to the TTB structure.[11] Among the large number of existing TTB structures, our attention is focused on mixed oxides within the $NaNbO_3$-WO_3 system. It has been reported for the composition corresponding to a 1:1 ratio ($NaNbWO_6$) that products obtained by the ceramic procedure exhibit complicated X-ray patterns that have been interpreted as a mixture of several

[a] Instituto de Ciencia de Materiales de Aragón, Universidad de Zaragoza – CSIC, Facultad de Ciencias, 50009 Zaragoza, Spain
[b] Departamento de Química, Universidad San Pablo – CEU, 28668 Boadilla del Monte, Madrid, Spain
Fax: +34-91-351-0496
E-mail: akuhn@ceu.es

phases,[12–14] and only a low-temperature route seems to be useful for obtaining TTB-like $NaNbWO_6$.[15] We recently reported the preparation of a TTB-like $NaNbWO_6$ single phase by the ceramic procedure,[16] although a more detailed analysis by electron diffraction revealed that this composition actually consists of two closely related tetragonal and monoclinic phases.[17]

$NaNbWO_6$, which can be regarded as a partially filled TTB with $x = 5$ when referred to $Na_xNb_5W_5O_{30}$, has been shown to undergo facile proton-exchange reactions,[16,17] and topotactic proton-exchange reactions with aqueous nitric acid solution lead to materials with the formula $Na_{1-y}H_yNbWO_6{\cdot}zH_2O$ ($0 < y \leq 0.46$; $0 \leq z \leq 0.12$). Additional interest is raised by the recent discovery of proton conduction in this type of TTB-like materials.[16,18]

Herein we report the synthesis of proton- and deuteron-exchanged derivatives of the *filled* TTB-like $Na_{1.2}Nb_{1.2}W_{0.8}O_6$ (or $Na_6Nb_6W_4O_{30}$ when referred to the unit cell), which has been called the F phase by Marinder.[10] Besides characterization of the exchanged products by means of XRD, electron diffraction (ED), and thermogravimetric analysis, we will pay special attention to the spectroscopic characterization by means of IR and Raman measurements in order to investigate the nature of the hydrogenated species formed upon exchange as this was not revealed by our previous ^1H NMR spectroscopic study on exchanged $Na_{1-y}H_yNbWO_6$.[17]

Results

Chemical and Structural Characterization of $Na_{1.2}Nb_{1.2}W_{0.8}O_6$ and the Exchanged Products

Elemental Analysis

Elemental analysis of the parent compound confirmed that the content of the different metals was close to nominal composition. Therefore, assuming that the oxygen content corresponds to the stoichiometric quantity, the formulation $Na_{1.2}Nb_{1.2}W_{0.8}O_6$ is used for the parent.

The Nb and W contents remain unchanged upon treatment with nitric acid, while the sodium content clearly decreases by around 65%. An empirical chemical formula of the exchanged product based on ICP results can be given as $H_{0.78}Na_{0.42}Nb_{1.2}W_{0.8}O_6$, assuming that the oxygen stoichiometry is maintained after the reaction and that an $Na^+ \leftrightarrow H^+$ exchange has effectively taken place (see below). The ability of $Na_{1.2}Nb_{1.2}W_{0.8}O_6$ to undergo proton-ion exchange reactions is higher than that of $NaNbWO_6$,[16] which has a related partially filled TTB-like structure. It has been shown that the sodium exchange rate of the latter is limited to half of the sodium ions and is only achieved after several consecutive exchange reactions. In $Na_{1.2}Nb_{1.2}W_{0.8}O_6$, however, approximately two out of the three sodium ions can be readily exchanged by a single treatment with dilute acid.

The ion exchange with deuterons yields the formula $D_{0.69}Na_{0.51}Nb_{1.2}W_{0.8}O_6$, as determined by chemical analysis.

X-ray Diffraction

Figure 2 shows the powder X-ray diffraction patterns of the TTB-like $Na_{1.2}Nb_{1.2}W_{0.8}O_6$ and an exchanged compound with formula $H_{0.78}Na_{0.42}Nb_{1.2}W_{0.8}O_6$, which was obtained after one treatment with nitric acid (see Experimental Section). The X-ray powder pattern of $Na_{1.2}Nb_{1.2}W_{0.8}O_6$ (Figure 2a) was successfully indexed in the tetragonal system, space group *P4/mbm* according to previously reported results.[10] The refined cell parameters of $Na_{1.2}Nb_{1.2}W_{0.8}O_6$ are $a = 12.2620(5)$, $c = 3.9199(2)$ Å, and the cell volume is 589.39(5) Å^3, all of which are in good agreement with previous reports.[19]

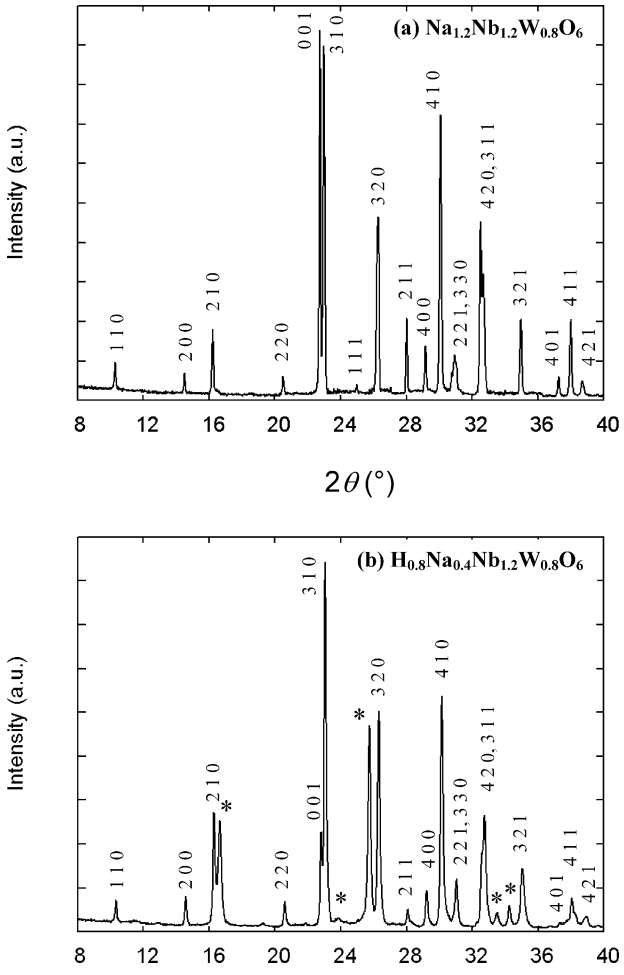

Figure 2. Powder X-ray patterns of: (a) $Na_{1.2}Nb_{1.2}W_{0.8}O_6$ and (b) the proton-exchanged product $H_{0.8}Na_{0.4}Nb_{1.2}W_{0.8}O_6$.

The powder X-ray diffraction pattern of $H_{0.78}Na_{0.42}Nb_{1.2}W_{0.8}O_6$ (Figure 2b) is similar to that of $Na_{1.2}Nb_{1.2}W_{0.8}O_6$, although the pattern also exhibits several additional diffraction lines that are not compatible with the basic TTB structure (marked as asterisks in Figure 2b).

ED Characterization

ED analysis performed on the parent $Na_{1.2}Nb_{1.2}W_{0.8}O_6$ revealed the well-known TTB structure type, in full agree-

ment with the results obtained from powder XRD. Figure 3 shows typical SAED patterns taken along the [001], [010], and [–1 1 –1] zone axes for comparison purposes.

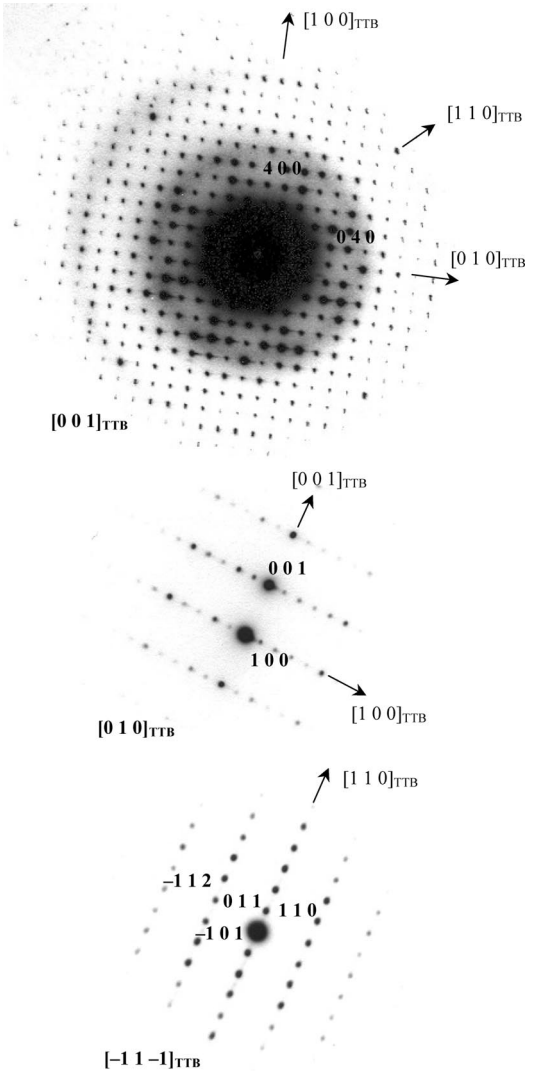

Figure 3. ED pattern along different zone axes for crystals of composition $Na_{1.2}Nb_{1.2}W_{0.8}O_6$. The spots are indexed based on the TTB cell ($a = b \approx 12.3$ Å; $c \approx 3.9$ Å).

ED analysis performed on an exchanged product with formula $H_{0.78}Na_{0.42}Nb_{1.2}W_{0.8}O_6$ showed the existence of a modulated structure, with similarities to the orthorhombic phase of $Ba_2NaNb_5O_{15}$.[20] Commensurate modulations are frequently observed in TTB-related structures due to octahedra tilt and/or cation order in the tunnels.[21–23] Initial attempts to describe the modulated TTB structure of the exchanged product observed by ED were made on the basis of orthorhombic supercells similar to those reported by Lin et al.[24,25] A systematic study of the reciprocal lattice was carried out for a series of SAED patterns in different zone axes, which are depicted in Figure 4. The SAED patterns always show the presence of modulation satellites, which were indexed on the basis of an orthorhombic supercell with $a \approx 2\sqrt{2}a_{TTB}$, $b \approx \sqrt{2}a_{TTB}$, and $c = 2c_{TTB}$. The orthorhombicity is characterized by the existence of a commensurate modulation along the $[110]_{TTB}$ direction, with a doubling of the c parameter. This cell is analogous to that previously described for several fluorides and oxides that adopt the TTB structure[23,25] as well as Pb_xWO_3.[22] The refined cell parameters from X-ray data using the orthorhombic supercell found by ED are: $a = 34.7630(7)$, $b = 17.3219(3)$, $c = 7.8465(1)$ Å.

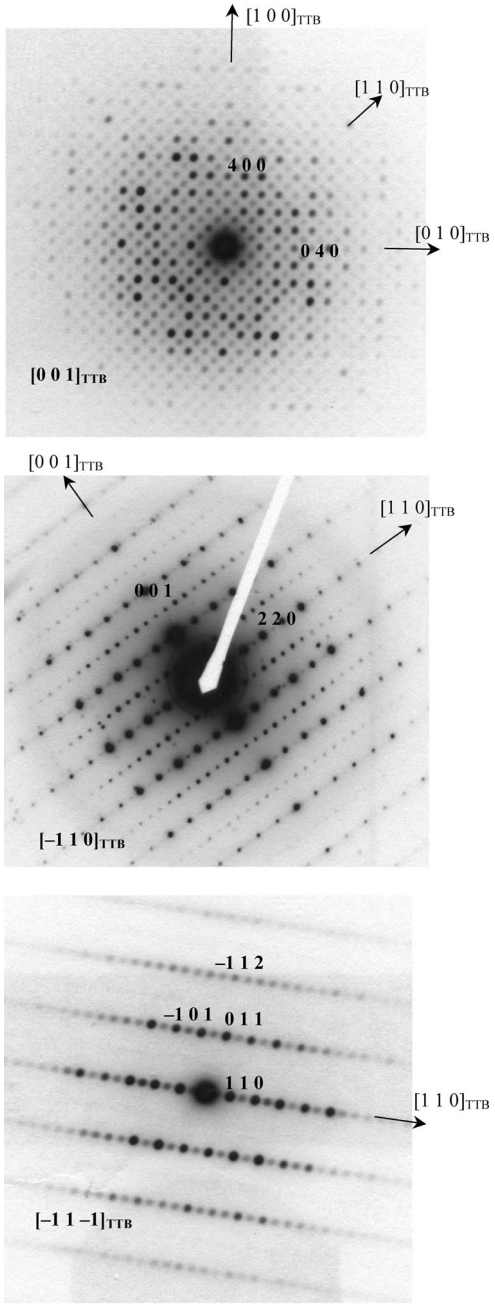

Figure 4. ED patterns along different zone axes for crystals of composition $H_{0.8}Na_{0.4}Nb_{1.2}W_{0.8}O_6$. The fundamental spots are indexed on the basis of the above simple TTB cell (see Figure 3).

The corresponding powder X-ray diffraction pattern of the deuteron-exchanged product $D_{0.69}Na_{0.51}Nb_{1.2}W_{0.8}O_6$ (not shown) was found to be practically identical to that of the protonated compound. Furthermore, the same modula-

tion satellites as in the above proton-exchanged product are observed in the ED patterns, in agreement with the aforementioned orthorhombic supercell. In summary, the X-ray and electron diffraction results confirm that the framework of the parent structure is basically maintained after the proton-exchange process. It can therefore be said that this ion-exchange reaction with TTB-type $Na_{1.2}Nb_{1.2}W_{0.8}O_6$ proceeds in a topotactical manner, as is also the case for ion-exchange reactions in TTB-like $NaNbWO_6$.[16,17]

The symmetry decrease from tetragonal to orthorhombic could be due to the existence of a cooperative tilting of the [Nb,WO_6] octahedron, as observed by Fabbrici et al.[23] for $K_{1-x}FeF_3$, which also has a TTB structure. Magnetic interactions between the iron ions in this fluoride are the origin of this tilting. In our case, the modulation is observed for the exchanged products but not for the parent. The possible shift of Nb or W from the center of the octahedron due to the presence of protons or deuterons in the tunnels has been investigated by Raman and IR spectroscopy (see below).

Thermal Analysis

The proton and deuteron contents were also investigated by means of thermal analysis. The results of the thermogravimetric experiments performed on a protonated and a deuterated sample are shown graphically in Figure 5. The thermal evolution of both protonated and deuterated series is dominated by two weight losses, located at around 200 and 580 °C, respectively, with the weight loss at about 200 °C being the most important. The weight losses observed between room temperature and 600 °C in the protonated and deuterated products are assigned to loss of water, according to the reactions:

$$H_xNa_{1.2-x}Nb_{1.2}W_{0.8}O_6 \rightarrow Na_{1.2-x}Nb_{1.2}W_{0.8}O_{6-x/2} + x/2\ H_2O$$

$$D_xNa_{1.2-x}Nb_{1.2}W_{0.8}O_6 \rightarrow Na_{1.2-x}Nb_{1.2}W_{0.8}O_{6-x/2} + x/2\ D_2O$$

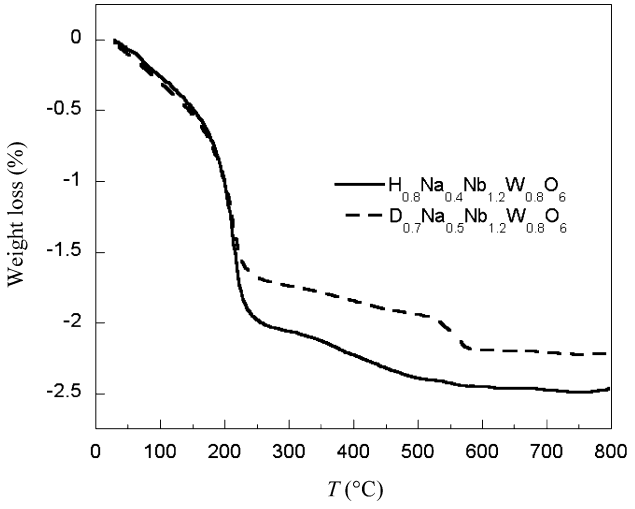

Figure 5. Weight loss of (a) the proton-exchanged compound $H_{0.8}Na_{0.4}Nb_{1.2}W_{0.8}O_6$ (solid line) and (b) the deuteron-exchanged compound $D_{0.7}Na_{0.5}Nb_{1.2}W_{0.8}O_6$ (dashed line) in the temperature range 25–800 °C.

The total hydrogen content in each sample was determined based on the above equations from the total weight loss observed in samples that had previously been dried under vacuum.

The weight losses calculated from thermogravimetric measurements yielded $x = 0.82$ for the protonated sample and $x = 0.68$ for the deuterated sample. These values are in excellent agreement with the corresponding values ($x = 0.78$ for H and $x = 0.68$ for D) deduced from the Na content, as obtained by ICP, if one assumes that the sodium deficiency is directly related to the quantity of protons or deuterons that are introduced in the bronze to equilibrate charge balance. For simplicity, the chemical compositions of the exchanged products obtained from elemental and thermal analysis are henceforth given as $H_{0.8}Na_{0.4}Nb_{1.2}W_{0.8}O_6$ and $D_{0.7}Na_{0.5}Nb_{1.2}W_{0.8}O_6$. Since two weight-loss steps are detected, two different proton or deuteron entities should be present in the exchanged products, similar to the partially filled TTB-like phase $NaNbWO_6$.[16,17]

The composition evolution regarding hydrogen and oxygen content was deduced from the weight loss found in the TG experiments after heating to different temperatures, according to the deprotonation reactions:

300 °C: $H_{0.8}Na_{0.4}Nb_{1.2}W_{0.8}O_6 \rightarrow H_{0.15}Na_{0.4}Nb_{1.2}W_{0.8}O_{5.67} + 0.33\ H_2O$

500 °C: $H_{0.8}Na_{0.4}Nb_{1.2}W_{0.8}O_6 \rightarrow H_{0.06}Na_{0.4}Nb_{1.2}W_{0.8}O_{5.63} + 0.37\ H_2O$

800 °C: $H_{0.8}Na_{0.4}Nb_{1.2}W_{0.8}O_6 \rightarrow Na_{0.4}Nb_{1.2}W_{0.8}O_{5.6} + 0.4\ H_2O$

and, for the deuterated compound:

300 °C: $D_{0.68}Na_{0.52}Nb_{1.2}W_{0.8}O_6 \rightarrow D_{0.16}Na_{0.52}Nb_{1.2}W_{0.8}O_{5.74} + 0.26\ D_2O$

500 °C: $D_{0.68}Na_{0.52}Nb_{1.2}W_{0.8}O_6 \rightarrow D_{0.11}Na_{0.52}Nb_{1.2}W_{0.8}O_{5.71} + 0.29\ D_2O$

800 °C: $D_{0.68}Na_{0.52}Nb_{1.2}W_{0.8}O_6 \rightarrow Na_{0.52}Nb_{1.2}W_{0.8}O_{5.66} + 0.34\ D_2O$

The parent composition is clearly not recovered after dehydration as uptake of oxygen is not possible due to the fact that both niobium and tungsten cannot be oxidized beyond their highest oxidation states.

Spectroscopic Characterization

Room-Temperature IR and Raman Measurements

The nature of the hydrogenated species was analyzed by performing a Raman and IR spectroscopic study of the parent and exchanged derivatives, with the aim of obtaining information regarding the H–O–H and OH groups. The most characteristic vibrational modes of these groups are a stretching mode, ν(OH), at 3500–3400 cm^{-1} and a bending mode, δ(HOH), at 1600 cm^{-1}. We recorded the FTIR spectra of $Na_{1.2}Nb_{1.2}W_{0.8}O_6$ and $H_{0.8}Na_{0.4}Nb_{1.2}W_{0.8}O_6$ after heating the samples under vacuum at 60 °C for 1 d in order to eliminate absorbed water. The TGA experiments did not show any weight loss at 80 °C. Figure 6 shows the FTIR spectra obtained for both the parent and protonated compounds.

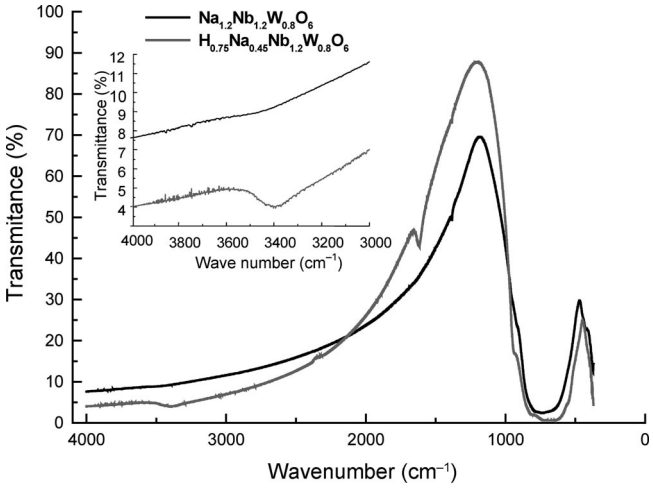

Figure 6. Transmittance FT-IR spectra of $Na_{1.2}Nb_{1.2}W_{0.8}O_6$ (black line) and $H_{0.8}Na_{0.4}Nb_{1.2}W_{0.8}O_6$ (grey line). The inset shows a magnification of the region between 3000 and 4000 cm^{-1}.

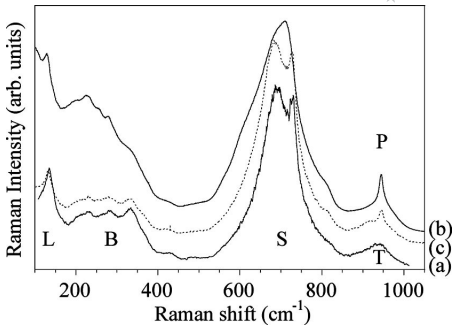

Figure 7. Room-temperature Raman spectra in the wavelength range 100–110 cm^{-1} of (a) $Na_{1.2}Nb_{1.2}W_{0.8}O_6$, (b) the protonated compound $H_{0.8}Na_{0.4}Nb_{1.2}W_{0.8}O_6$, and (c) the deuterated compound $D_{0.7}Na_{0.5}Nb_{1.2}W_{0.8}O_6$.

The spectrum of the non-protonated sample shows only a broad and strong absorption centered at about 800 cm^{-1}, which is assigned to the internal modes of the [Nb/WO_6] octahedra. However, additional absorption bands are observed for the protonated sample: (1) a broad absorption centered at 3400 cm^{-1}, which corresponds to the ν(OH) stretching mode, and (2) another medium absorption at 1615 cm^{-1} that corresponds to the δ(HOH) bending mode. The absence of a dehydration stage below 100 °C in the TGA measurements implies that no adsorbed water is present in our samples, therefore the detection of ν(O–H) and δ(H–O–H) absorptions must be attributed to protons being trapped in pairs close to the oxygen ions and forming coordinated OH_2 entities somewhere in the tunnels.

Figure 7 shows the room-temperature Raman spectrum of the parent compound $Na_{1.2}Nb_{1.2}W_{0.8}O_6$ (a), as well as those of the proton- and deuteron-exchanged materials with formulations $H_{0.8}Na_{0.4}Nb_{1.2}W_{0.8}O_6$ (b) and $D_{0.7}Na_{0.5}Nb_{1.2}W_{0.8}O_6$ (c), respectively, from 100 to 1100 cm^{-1}. None of these compounds show any other bands above 1100 cm^{-1} up to 4000 cm^{-1}, therefore the bands corresponding to the ν(OH) stretching mode and the δ(HOH) bending mode seem to be too weak to be observed. Nevertheless, a detailed analysis of the low-frequency region of the Raman spectra provided additional information on the nature of the hydrogenated species through its influence on the modes of the M–O framework.

The main features of the spectrum of the parent compound (Figure 7a) are as follows. Below 500 cm^{-1}, we find a narrow band (L) at 135 cm^{-1} and a group of overlapping bands (B) extending from 200 to 450 cm^{-1}. Two well-separated bands are observed above 500 cm^{-1}: a strong band (S), which extends from 500 to 850 cm^{-1} and is clearly composed of several sub-bands, and a high-frequency band (T), which extends from 850 to 1000 cm^{-1} and also contains more than one component. The lack of polarization measurements as well as the intrinsic disorder of the structure due to Nb/W disorder preclude a precise attribution of the bands. Qualitatively, however, as is usual in the study of framework structures consisting of [MO_6] octahedral units, we can interpret the vibrational spectrum in terms of internal modes of the [MO_6] octahedra and external (or lattice) modes, including cation translations and/or octahedra librations.[26–29] We can therefore attribute the bands appearing in the region 200–400 cm^{-1} to O–M–O bending vibrations, as well as to Na vibrations; the narrow band L might be due to heavier cation vibration or, more probably, to libration of the [MO_6] octahedra. By analogy with many other Nb and W oxides, the strong band (S) centered around 700 cm^{-1} is attributed to the stretching vibration of the M–O bonds. The presence of another band at higher frequency (band T) in the Raman or IR spectra is characteristic of very short M–O bonds to high-valence cations such as Nb^{V}, W^{VI}, Mo^{VI}, etc., which are usually denoted as M=O and named terminal.[27–33]

The spectra of the parent and exchanged compounds have many features in common, thus indicating, in agreement with the XRD results, that the structure is basically preserved upon ion exchange. Some striking differences are evident in the high-frequency region, however, in particular a narrow and intense peak (P) that develops in the protonated sample at 944.5 cm^{-1} and is superposed on the broad band T centered at around 950 cm^{-1}. Other differences are also found in the protonated sample, such as the presence of a shoulder at about 620 cm^{-1}, as well as other minor changes in the low-frequency region.

In order to verify whether any of the bands (especially band P) involve the vibration of any hydrogen species introduced in the sample, we investigated the deuterated analogue of the proton-exchanged compound. Figure 7(c) shows the Raman spectrum of this sample, which is intermediate between those of the parent and proton-exchanged samples in the sense that it shows band P at the same position as in the protonated sample but all the other bands are closer to those of the parent compound. We shall discuss the differences between the room-temperature spectra of protonated and deuterated samples below. For our purposes, the appearance of band P and the absence of any new bands at lower frequency indicate that no isotope effect

occurs, and that band P therefore does not involve hydrogen vibration in any of its forms.

Temperature Evolution of the Raman Spectrum

We performed two kinds of Raman experiments to further elucidate the nature of the hydrogen species formed upon ion exchange and the mechanism of the dehydration stages, namely variable-temperature experiments, with the temperature increasing from room temperature to 500 °C, and measurements at room temperature of samples previously heated to 300, 500, and 800 °C, in parallel with the TG experiments described in previous sections.

Figure 8(a) shows the temperature evolution of the Raman spectrum of the proton-exchanged compound in the 400–1100 cm^{-1} frequency region. Several aspects can be noted from this evolution. First of all we note that there is no change in the Raman spectra at 80–100 °C, which is the region where adsorbed water, if present, would be lost. As the temperature increases, the intensity of the high-frequency bands (S and T) decreases gradually, reaching a minimum at $T \approx T_p$ = 170 °C, and then increases again up to values even higher than at room temperature. In parallel with the intensity variation, peak P decreases in intensity until it vanishes at $T \approx T_p$, while the broad band underneath, which extends from 900 to 1000 cm^{-1}, remains with the same intensity relative to the rest of the spectrum. The shoulder at 620 cm^{-1} also disappears at T_p, thus indicating that it is also related to proton insertion. These changes are irreversible: neither peak P nor the shoulder at 620 cm^{-1} are recovered after cooling the sample down to room temperature after heating. No remarkable change is observed in the low-frequency region (not shown), which suggests that the basic framework is preserved throughout the deprotonation process.

The evolution of the high-frequency spectrum of the deuterated sample is shown in Figure 8(b). As in the protonated case, peak P disappears at a temperature that is, within experimental resolution, the same as in the protonated case (170 °C). The intensity decrease/increase sequence is also found, although it is less pronounced in this case.

The parent compound shows a much smoother evolution (not shown), and the intensity decrease/increase sequence of the high-frequency bands is not observed. The absence of peak P in the spectrum of the parent compound, the temperature evolution of the high-frequency spectrum, as well as the close coincidence of T_p with the first mass-loss stage in the TGA experiments indicate that band P is associated with the insertion of protons in the lattice and that its disappearance at T_p is due to a deprotonation process.

The Origin of Peak P

Once we have excluded the vibration of hydrogen species, in any of their forms, as the origin of the 944.5-cm^{-1} band, we are left with few other possibilities. As noted above, the frequency is typical of the short M–O bonds that have been reported to appear in several situations, some of which are discussed here:

(i) Cation-valence disorder arising from the substitution of high-valence cations by lower valence ones.[34] In our case, the structure contains two aliovalent disordered cations (W^{6+} and Nb^{5+}) in both the parent and the exchanged compounds. We suggest that this mechanism may contribute to the broad band T, which is already present in the parent compound, but does not explain the appearance of peak P upon proton or deuteron exchange.

(ii) Oxygen or cation vacancies, as in pyrochlore WO_3[35] or hexagonal $A_yB_xW_{3-x}O_9$ bronzes.[27] In our case, we note that band P is formed upon proton exchange with Na^+ without the detection of cation non-stoichiometry or of any cation-valence change that may indicate oxygen deficiency.

(iii) Terminal bonds in grain boundaries[36] is another possibility. As in the preceding point, although these bonds are indeed expected to form, there is no reason why they would be particularly activated upon protonation.

(iv) Terminal bonds in layered hydrates, such as $WO_3{\cdot}nH_2O$ or $MoO_3{\cdot}nH_2O$.[30–32,37] The trapping of two protons close to a terminal oxygen atom in the interlayer space, to yield a coordinated water molecule, results in a long M–O bond with the oxygen atom participating in the water molecule, and a short (terminal) M=O bond in the opposite direction. In our case, the TTB structure does not present such an

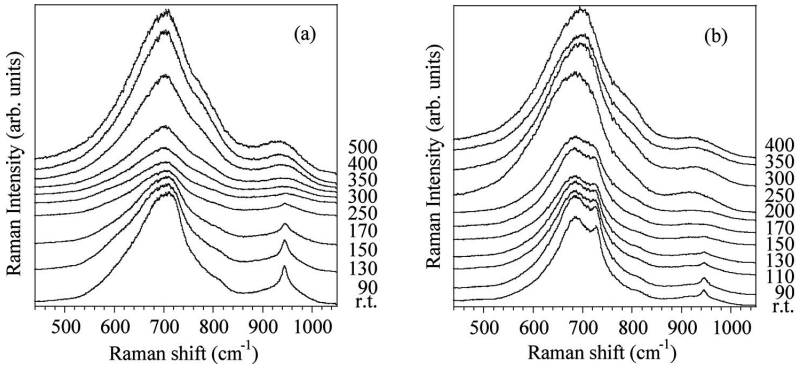

Figure 8. Temperature evolution of the Raman spectrum of the proton- (a) and deuteron-exchanged (b) compounds. The spectra have been shifted vertically for presentation purposes.

inter-layer space or terminal oxygen atoms since all MO_6 octahedra are corner-linked in all three directions. However, the effect could be similar if two protons located in a tunnel interact with the oxygen atom. A plausible explanation for band P may therefore be the shortening of W–O or Nb–O bonds due to the trapping of protons somewhere in the tunnels, which results in the shift of the M cation and the deformation of the MO_6 octahedra. We shall use the notation M=O to refer to the short metal–oxygen distance.

Whether the protons are isolated or in pairs, as well as their precise location, cannot be ascertained by Raman spectroscopy, although the information obtained from the IR spectra suggests that the protons form pairs. Assuming that the short M=O bond is mainly due to the shift of the central cation, a long M–O bond should be formed in parallel with the short one; we tentatively assign the shoulder at about 620 cm^{-1} to this long M–O bond.

Raman Measurements at Room Temperature of Samples Heated up to 300, 500, and 800 °C

We have shown in a previous section, through variable-temperature measurements, that peak P disappears at around 170 °C in both the proton- and deuteron-exchanged compounds but that no new bands or relevant changes are detected beyond that temperature, at least up to 500 °C. On the other hand, TG experiments (see Figure 5) show that dehydrogenation occurs in two steps: a narrow one between 170 and 200 °C, which coincides with the disappearance of peak P in the Raman spectra, and another smooth one, which extends up to temperatures as high as 500 and 570 °C, for proton- and deuteron-containing compounds, respectively. This means that some kind of hydrogen species is still present between 200 and 500–600 °C. Since spectral broadening is large at those temperatures, it might be the case that new bands are formed but are undetectable in the high-temperature Raman measurements. Therefore, and in order to clarify the nature of the dehydrogenation stages, we performed Raman measurements at room temperature of samples heated to 300, 500, and 800 °C in parallel with the TG experiments reported above.

These spectra are presented in Figures 9(a) and (b) for proton- and deuteron-exchanged compounds, respectively, together with those of the parent materials. As expected, peak P, which was attributed in the preceding section to short M=O bonds formed upon hydrogenation, disappears in the samples heated to 300 °C (labeled as H-300 and D-300 in Figure 9) and above, although no new band develops in samples heated to 300 or 500 °C (labeled as H-300/H-500 and D-300/D-500 in Figure 9) that might be attributed to new hydrogen species. The only change observed upon increasing the treatment temperature is a broadening of the spectrum, which results in a loss of peak resolution. The evolution of the spectra shown in Figures 9(a) and (b) suggests that the spectral broadening is related to the proton or deuteron content. The broadening of all bands in the proton-exchanged sample, which is already remarkable in the parent sample, increases in the protonated sample heated at 300 °C (H-300 in Figure 9), which still contains some amount of proton species, and tends to decrease for the protonated samples heated at 500 and 800 °C (H-500 and H-800, respectively, in Figure 9), in other words as the second stage of deprotonation is reached and passed. The broadening in the deuteron-exchanged compound, which is small even in the as-grown sample, increases slightly in the deuterated sample heated at 300 and 500 °C (D-300 and D-500, respectively, in Figure 9) and finally falls for the deuterated sample heated at 800 °C (D-800 in Figure 9). To clarify this behavior, we show in Figure 10 the width of a representative band ($\tilde{\nu} \approx 730$ cm^{-1}), obtained by a decomposition of the spectrum as a sum of Lorentzian profiles, as a function of the temperature at which the sample has been heated in the TG experiments. Other bands show a similar trend. The numbers accompanying each point represent the hydrogen content per formula determined by TGA and the vertical lines indicate the approximate temperatures of the dehydration steps. The width of the band in the non-exchanged material is also included for comparison.

First, we note that both the proton- and deuteron-exchanged samples reach a similar width after dehydration and that this width is also similar to that of the non-ex-

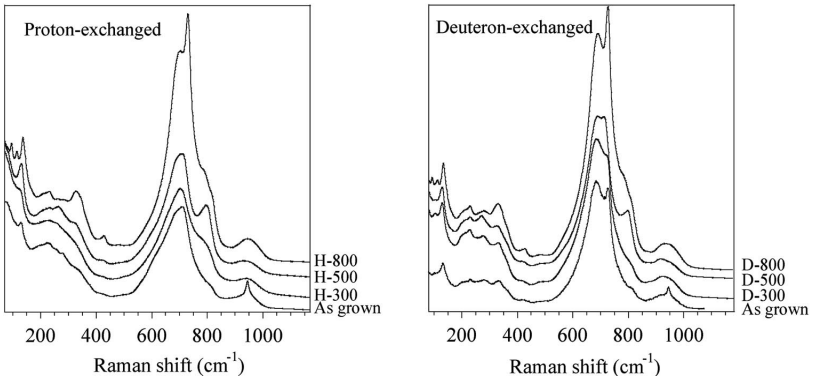

Figure 9. Room-temperature Raman spectrum of the proton- (a) and deuteron-exchanged (b) compounds thermally treated at room temperature, 300, 500, and 800 °C. The spectra have been shifted vertically for presentation purposes.

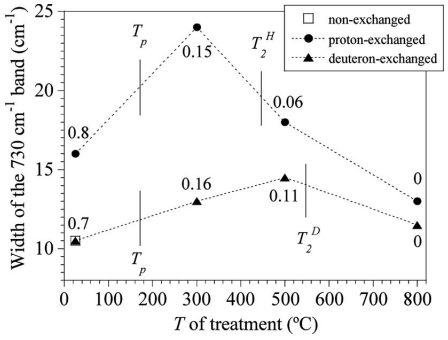

Figure 10. Full width of the band observed at about 730 cm^{-1} as a function of the temperature reached in the TG experiments. The stages of thermal dehydration are indicated by vertical lines. The remaining hydrogen content per $H_xNa_{1.2-x}Nb_{1.2}W_{0.8}O_6$ formula is given close to each datum.

changed material. This means that the structural disorder arising from the sodium and oxygen vacancies is not the most relevant factor in producing spectral broadening. The maximum broadening is not reached for the samples with maximum hydrogen content but for samples heated to temperatures above the first dehydration step, where most of the protons or deuterons are lost. Once again, this means that the majority of protons or deuterons are not relevant to the spectral broadening. Our hypothesis is that broadening is not related to the total hydrogen content but to the presence of mobile protons or deuterons. Assuming that the broadening has a dynamic origin, we conclude that most of the protons or deuterons are not mobile at room temperature, whereas the hydrogen entities remaining after the first dehydration step are mobile and thus broaden the spectrum. The fact that the spectrum of the as-prepared proton-exchanged material is already broad means that a certain amount of the protons are mobile in this sample. The progressive narrowing of the spectrum for protonated samples heated to 500 and 800 °C parallels the decrease of proton content.

The broadening is smaller in the deuterated samples, in agreement with both the lower deuteron concentration and the lower deuteron mobility. The hypothesis that the broadening has a dynamic origin explains, in particular, why the spectrum of the as-prepared deuterated sample looks similar to that of the non-exchanged material despite having a deuterium content (0.7 atoms/formula) that is not too far from that of the proton-exchanged compound (0.8). No mobile deuterons exist at room temperature in the deuterated compound. Since some broadening is observed for deuterated samples heated at 300 and 500 °C, we conclude that some of the deuterons released at T_p are retrapped in the form of mobile entities.

The differences between the spectra of proton- and deuteron-exchanged samples tend to disappear upon increasing the measurement or thermal-treatment temperature. In high-temperature measurements (Figure 8), the spectra above 250 °C look very similar for both kinds of samples. For thermally treated samples (Figure 9), it is clear that differences are still observed between the protonated and deuterated samples heated at 300 °C, although these differences decrease when comparing the spectra of the protonated and deuterated samples heated at 500 °C and are almost negligible in samples heated to 800 °C, when protons or deuterons are completely lost. The end compounds, namely the protonated and deuterated samples heated at 800 °C, show very similar, TTB-like spectra, which indicates that both materials reach the same end structure after total proton or deuterium loss and that this structure is still TTB-like.

Discussion

The exchange of Na by a proton (or deuteron) has been shown to occur in TTB-like $Na_{1.2}Nb_{1.2}W_{0.8}O_6$ up to an extent of about 65% of total Na. As regards the precise proton location, we note that the fact that they enter the lattice through ion exchange for Na^+ does not imply that they occupy the empty sites left by mobile sodium ions. In any case, protons will likely prefer non-centered sites within the tunnels, close to the oxygen ions. This results in an oxygen–proton interaction that is detectable by IR spectroscopy. The presence of a broad and weak band at 3400 cm^{-1} [$\nu(OH^-)$ stretch] indicates the presence of OH groups. The IR spectra also exhibit a band characteristic of a δ(HOH) bending mode at 1615 cm^{-1}, which may correspond to coordinated water formed by a couple of protons interacting with the oxygen atoms of the W/Nb–O framework. The Raman results strongly support this possibility through the appearance of a band at 944.5 cm^{-1}, which has been attributed to the shortening of some M–O bonds due to the trapping of protons close to an oxygen ion.

The first stage of mass loss observed by TGA at about 170 °C is clearly reflected in the Raman spectrum through the disappearance of the bands at 944.5 and 620 cm^{-1}. No new bands are detected above that temperature, and the spectrum evolves regularly up to 500 °C. In particular, no change is detected at the temperature of the second stage of mass loss in the TGA experiments (approx. 500 °C). The ensemble of spectroscopic and TGA results as a function of temperature point to the occurrence of a deprotonation through the reaction already pointed out in the Results section:

$$H_xNa_{1.2-x}Nb_{1.2}W_{0.8}O_6 \rightarrow Na_{1.2-x}Nb_{1.2}W_{0.8}O_{6-x/2} + x/2\ H_2O$$

According to this mechanism, water molecules are formed by the released protons together with oxygen atoms from the lattice, which leads to an oxygen-deficient system.

A detailed examination of the spectra of the thermally treated samples suggests either that two different hydrogen entities are formed or that protons enter into two different locations in one of which (the majority one) the protons are fixed at room temperature and are released at T_p, together with lattice oxygen atoms, in the form of water molecules. A minority of them, however, are mobile even at room temperature. Mobile protons are involved in the second stage of mass loss that occurs above 400 °C.

Electron diffraction experiments, as well as Raman spectra, show that two kinds of structural changes occur upon ion exchange, namely an MO_6 octahedra tilt that yields a modulated orthorhombic structure with $a \approx 2\sqrt{2}a_{TTB}$, $b \approx \sqrt{2}a_{TTB}$, and $c = 2c_{TTB}$, and a cation shift within the octahedral cage to form short M=O bonds. Superlattice modulations are very common in TTB-like compounds and are usually attributed to the presence of cation ordering, octahedron tilt, or both. At this point we propose a model that explains, at least in a qualitative way, the origin of the superstructure. This model is based on the hypothesis that the structural changes occurring in the proton-exchanged compound are not due to the presence of protons themselves but to the combined effect of octahedra tilt and Na/vacancy ordering in the pentagonal tunnels. The basic assumption is that Na cations and vacancies alternate along the *c* axis, a tendency that has already been proposed for Na_xWO_3 by Takusagawa and Jacobson.[7] This yields the doubling of the *c* parameter. Different schemes of cation ordering in the *ab* plane result in different types of structural modulation, one of which is the $2\sqrt{2}a_{TTB} \times \sqrt{2}a_{TTB} \times 2c_{TTB}$ modulation discussed previously for Pb_xWO_3.[22] The Na/vacancy ordering would also explain the existence of Na that cannot be exchanged and remains in the pentagonal tunnels (two ions per unit cell formula). In that case the end composition would be $Na_2H_4Nb_6W_4O_{30}$, which is very close to the experimental one.

The most likely proton location within this model would be in the vacant pentagonal cavities, in pairs, forming OH_2 coordinated water molecules and giving rise to short and long M–O bonds. This means that all the pentagonal sites will be filled in the protonated material, either by Na ions or by pairs of hydrogen ions. The disappearance of the P band upon deprotonation, which is discussed in detail in the Results section, implies that the M cation recovers its regular position when protons are lost.

Conclusions

Proton- and deuteron-exchange reactions have been performed on TTB-type $Na_{1.2}Nb_{1.2}W_{0.8}O_6$. Na^+/H^+ and Na^+/D^+ exchanges occur when aqueous nitric acid solutions are used as the exchanging agent. These reactions yield crystalline powder samples. Approximately two out of three Na^+ ions can be exchanged under the selected experimental conditions with retention of the basic TTB skeleton framework, as shown by X-ray diffraction. A more detailed study by means of ED techniques has shown that the extra diffraction lines observed in the exchanged material are due to the occurrence of an orthorhombic superstructure to the basic TTB-like structure with $a \approx 2\sqrt{2}a_{TTB}$, $b \approx \sqrt{2}a_{TTB}$, and $c = 2c_{TTB}$. Distortions and tilts of the MO_6 framework, which are connected to the presence of protons in the tunnels of the TTB structure, have been proposed as the origin of the commensurate modulation in ion-exchanged products. The nature of the hydrogenated species has been analyzed by means of IR and Raman spectroscopy carried out on both parent and exchanged compounds, and the results have been interpreted in terms of short M–O (M = Nb or W) bonds formed through the trapping of two protons or deuterons close to the oxygen ions of the $[MO_6]$ octahedra.

The spectroscopic measurements with partially dehydrated samples suggest that two different hydrogen entities are formed. The majority of these species are non-mobile at room temperature and disappear at 170 °C, while a minority of them are mobile and remain at, or are formed above, T_p.

Experimental Section

Chemical Synthesis: $Na_{1.2}Nb_{1.2}W_{0.8}O_6$, was prepared by a two-step reaction. The precursor $NaNbO_3$ was prepared by finely grinding a mixture of Na_2CO_3 (Aldrich, 99.95%) and Nb_2O_5 (Aldrich, 99.9%), which was then pressed and heated at 850 °C for 24 h. In a second step, stoichiometric amounts of the as-prepared $NaNbO_3$ and WO_3 (Aldrich, >99%) were pressed into pellets and heated at 950 °C for 48 h. At the end of the heating period the sample was quenched in liquid nitrogen in order to avoid phase segregation. This procedure was repeated once using the same conditions in order to ensure the homogeneity of the sample. Proton exchange was carried out with dilute nitric acid (5 M) as the exchanging agent. Powdery $Na_{1.2}Nb_{1.2}W_{0.8}O_6$ was refluxed at 80 °C in dilute nitric acid (molar ratio of oxide/HNO_3 = 1:20) for 24 h. The product obtained was isolated by centrifugation and washed first with water and then with acetone. Finally, it was dried under vacuum. A deuterated product was prepared according to the same procedure but with 5 M DNO_3 in D_2O solution as the exchanging agent. However, in this case the procedures were carried out with outgassed sample and solvents, under an inert gas, using standard Schlenk techniques. The solid obtained was filtered off, washed with degassed D_2O, and finally dried under vacuum

Structural Characterization: The phase purity of both parent and ion-exchanged materials was checked by means of powder X-ray diffraction measurements carried out with a Bruker D8 high-resolution X-ray powder diffractometer equipped with a position-sensitive detector (PSD; MBraun PSD-50M) using monochromatic Cu-$K_{\alpha 1}$ (λ = 1.5406 Å) radiation obtained with a germanium primary monochromator. Refinements of cell parameters were made with a least-squares fit using the WinPLOTR program.[38] Data collection was performed in 0.02° steps with counting times ranging from 3 to 10 s. Electron diffraction (ED) was carried out using a Philips FEG200 transmission electron microscope operating at 200 kV. The specimens were prepared by grinding the powder in *n*-butyl alcohol and concentrating the suspension on a copper grid covered with a holey carbon film.

Chemical Analysis: The metal contents of both parent and proton-exchanged samples were determined by inductively coupled plasma atomic emission spectroscopy (ICP-AES) using a Perkin–Elmer apparatus. The hydrogen content was determined by thermal analysis. Thermogravimetric analyses were performed with a Seiko instrument TG/DTA 6200 apparatus in the temperature range 25–650 °C under an argon flow. The heating and cooling rates were set to 10 °C min^{-1}.

Spectroscopic Characterization: IR spectra were recorded with an FTIR Perkin–Elmer 599 spectrometer working in the 4000–400 cm^{-1} spectral range in a classical transmission configuration. The resolution was 4 cm^{-1}. Samples were dried at 60 °C under vac-

uum to eliminate moisture, then diluted with KBr and pelletised. Raman measurements were performed with a DILOR XY spectrometer equipped with a diode array detector, using the 514.5-nm line of an Ar^+ laser. The spectral resolution was typically 3 cm^{-1}. A Linkam TP91 unit was used for measurements between room temperature and 500 °C.

Acknowledgments

This work was supported financially by the Spanish MEC through the projects MAT2004-03070-C05-01 and MAT2004-03070-C05-03, the Comunidad de Madrid (S-0505/PPQ/0358), and the Universidad San Pablo-CEU.

[1] A. Magnéli, *Ark. Kemi* **1949**, *1*, 213–221.
[2] C. J. Raub, S. Broadsto, B. T. Matthias, M. A. Jensen, A. R. Sweedler, *Phys. Rev. Lett.* **1964**, *13*, 746–747.
[3] P. G. Dickens, D. J. Murphy, T. K. Halstead, *J. Solid State Chem.* **1973**, *6*, 370–373.
[4] B. Gérand, G. Nowogrocky, J. Guenot, M. Figlarz, *J. Solid State Chem.* **1979**, *29*, 429–434.
[5] M. Figlarz, *Prog. Solid State Chem.* **1989**, *19*, 1–46.
[6] K. S. Rao, K. H. Yoon, *J. Mater. Sci.* **2003**, *38*, 391–400.
[7] F. Takusagawa, R. A. Jacobson, *J. Solid State Chem.* **1976**, *18*, 163–174.
[8] T. Ikeda, T. Haraguchi, Y. Onodera, T. Saito, *Jpn. J. Appl. Phys.* **1971**, *10*, 987–994.
[9] L. Kihlborg, R. Sharma, *J. Microsc. Spectrosc. Electron.* **1982**, *7*, 387–396.
[10] B.-O. Marinder, *Chem. Scr.* **1986**, *26*, 547–560.
[11] M. Sundberg, B.-O. Marinder, *J. Solid State Chem.* **1990**, *84*, 23–38.
[12] Y. Bouillaud, F. Bonnin, *Bull. Soc. Fr. Miner. Crist.* **1965**, *88*, 700–701.
[13] G. Blasse, A. D. M. dePauw, *J. Inorg. Nucl. Chem.* **1970**, *32*, 3960–3961.
[14] O. B. Thakre, V. S. Chincholkar, *Curr. Sci.* **1972**, *41*, 735–736.
[15] C. Michel, D. Groult, A. Deschanvres, B. Raveau, *J. Inorg. Nucl. Chem.* **1975**, *37*, 251–255.
[16] A. Kuhn, H. Bashir, A. L. Dos Santos, J. L. Acosta, F. Garcia-Alvarado, *J. Solid State Chem.* **2004**, *177*, 2366–2372.
[17] A. Kuhn, M. T. Azcondo, U. Amador, K. Boulahya, I. Sobrados, J. Sanz, F. García-Alvarado, *Inorg. Chem.* **2007**, *46*, 5390–5397.
[18] E. Kendrick, M. S. Islam, P. R. Slater, *Solid State Ionics* **2005**, *176*, 2975–2978.
[19] T. Horlin, B.-O. Marinder, M. Nygren, *Rev. Chim. Miner.* **1982**, *19*, 231–238.
[20] S. Singh, D. A. Draegert, J. E. Geusic, *Phys. Rev. B* **1970**, *2*, 2709–2724.
[21] S. K. Haydon, D. A. Jefferson, *J. Solid State Chem.* **2001**, *161*, 135–151.
[22] S. K. Haydon, D. A. Jefferson, *J. Solid State Chem.* **2002**, *168*, 306–315.
[23] S. Fabbrici, E. Montanari, L. Righi, G. Calestani, A. Migliori, *Chem. Mater.* **2004**, *16*, 3007–3019.
[24] P. J. Lin, L. A. Bursill, *Acta Crystallogr., Sect. B* **1987**, *43*, 504–512.
[25] P. Labbé, H. Leligny, B. Raveau, J. Schneck, J. C. Toledano, *J. Phys. Condens. Matter* **1989**, *2*, 25–43.
[26] H. R. Xia, H. C. Chen, H. Yu, K. X. Wang, B. Y. Zhao, *Phys. Status Solidi B* **1998**, *210*, 47–59.
[27] M. Maczka, A. G. Souza, P. T. C. Freire, J. Mendes, S. Kojima, J. Hanuza, A. Majchrowski, *J. Raman Spectrosc.* **2003**, *34*, 199–204.
[28] M. Maczka, J. Hanuza, A. Majchrowski, *J. Raman Spectrosc.* **2001**, *32*, 929–936.
[29] M. Maczka, J. Hanuza, S. Kojima, A. Majchrowski, *J. Raman Spectrosc.* **2001**, *32*, 287–291.
[30] C. Guéry, C. Choquet, F. Dujeancourt, J. M. Tarascon, J. C. Lassegues, *J. Solid State Electrochem.* **1997**, *1*, 199–207.
[31] M. F. Daniel, B. Desbat, J. C. Lassegues, B. Gérand, M. Figlarz, *J. Solid State Chem.* **1987**, *67*, 235–247.
[32] N. Sotani, T. Manago, T. Suzuki, K. Eda, *J. Solid State Chem.* **2001**, *159*, 87–93.
[33] J. L. Paul, J. C. Lassegues, *J. Solid State Chem.* **1993**, *106*, 357–371.
[34] R. Mattes, M. Leimkuhler, A. Nagel, *Z. Anorg. Allg. Chem.* **1990**, *582*, 131–142.
[35] A. Coucou, A. Driouiche, M. Figlarz, M. Touboul, G. Chevrier, *J. Solid State Chem.* **1992**, *99*, 283–289.
[36] A. Kuzmin, J. Purans, E. Cazzanelli, C. Vinegoni, G. Mariotto, *J. Appl. Phys.* **1998**, *84*, 5515–5524.
[37] S. Crouchbaker, P. G. Dickens, *Polyhedron* **1986**, *5*, 63–66.
[38] *WinPLOTR: A Windows tool for powder diffraction pattern analysis*: T. Roisnel, J. Rodriguez-Carvajal, *Materials Science Forum, Proceedings of the Seventh European Powder Diffraction Conference (EPDIC 7)* (Eds.: R. Delhez, E. J. Mittenmeijer), **2000**, p. 118–123.

Received: July 5, 2007
Published Online: November 8, 2007

